THE ASTROPHYSICAL JOURNAL, 355:190–196, 1990 May 20

RADIATIVE TRANSFER MODELING OF RADIO-FREQUENCY SPECTRAL LINE DATA: ACCRETION ONTO G10.6−0.4

E. R. KETO
Institute of Geophysics and Planetary Physics, Lawrence Livermore National Laboratory
Received 1989 February 21; accepted 1989 November 27

ABSTRACT

In this paper we describe a procedure for simulating spectral line images of three-dimensional molecular clouds. We suggest how this technique can be useful in the more general problem of determining the three-dimensional structure of molecular clouds. We demonstrate our technique by comparing observed and simulated images of the accretion flow associated with high-mass star formation in the region G10.6−0.4. We describe, as a result of the comparison, the temperature, density, and velocity fields and present a vector map of the accretion flow direction and magnitude. Our results indicate that the molecular cloud core is strongly condensed and has approximately equal velocities in rotation and infall at its current evolutionary state. The rapid collapse and lack of rotational support suggests that significant angular momentum transfer is occurring over scales at least as large as those observed (0.5 pc). A milligauss magnetic field would have sufficient energy to supply the required braking torque of 10^{47} ergs.

Subject headings: nebulae: H II regions — nebulae: individual (G10.6−0.4) — radiative transfer — radio sources: lines

I. INTRODUCTION

The recent successes of multielement interferometers, the Very Large Array, and the Hat Creek and Owens Valley Observatories in detecting and resolving the velocity structure in gravitationally bound gas about different galactic sources, the Galactic center (Gusten *et al.* 1987), high-mass stars (Ho and Haschick 1986), and low-mass stars (Sargent and Beckwith 1988) suggests that a means of comparing observations with detailed physical models may prove helpful in determining the three-dimensional internal structure of such molecular cloud flows. Simple techniques of spectral line analysis depend on assuming conditions of uniform source structure so that the radiative transfer equation can be solved analytically. Such an approach does not allow an investigation of the three-dimensional structure of the source. In principle, this information is contained in the data, since except for the most optically thick gas, the line brightness represents an integral average over the entire line of sight through the cloud. In § III we describe a program which captures the essential physics of line generation in a molecular cloud and for given velocity, temperature, and density fields, produces a spectral line data base from which images can be produced and compared with the observed images.

In § IV, to illustrate the capability of this technique in reproducing observed images, we compare simulated images from a model of an accretion flow with VLA observations of the molecular gas around G10.6−0.4. We describe several aspects of the model in considerable detail. The model is mathematically simple and has been arbitrarily chosen to provide an apparent match to the observations consistent with the physics of accretions flows. The model allows us to refine our understanding of the structure of G10.6−0.4 and to present for the first time a map of the vector velocities in the accretion flow.

II. RADIATIVE TRANSFER

For comparison of any model with observations, we need to compute a three-dimensional image of the line brightness where two of the three dimensions are the x and y map positions and the third is the line-of-sight velocity. We adopt the following simple scheme. From the H_2 density, temperature, and fractional abundance of our molecular tracer, we compute the source function and opacity, assuming the populations in the line transition quantum states are in LTE. The local line profile is specified by the thermal and turbulent broadening and the line-of-sight velocity. The line brightness at a particular frequency v and position x, y may then be determined by integrating the radiative transfer equation along the line of sight:

$$\frac{\partial I(x, y, z, v)}{\partial z} = \alpha(x, y, z, v)[S(x, y, z) - I(x, y, z, v)] , \quad (1)$$

where $I(x, y, v)$ is the line brightness as a function of sky position (x, y) and frequency v. The source function S is

$$S(x, y, z) = \frac{A_{ul}\, n_u(x, y, z)}{g_l\, n_l(x, y, z) - g_u\, n_u(x, y, z)} , \quad (2)$$

the absorption coefficient α is

$$\alpha(x, y, z, v) = \frac{hv}{4\pi}\,[n_l(x, y, z)B_{lu} - n_u(x, y, z)B_{ul}]\phi(x, y, z, v) , \quad (3)$$

and the line profile function ϕ is

$$\phi(x, y, z, v) = \frac{1}{\sqrt{\pi}\,\Delta v}\, e^{[v - (v_0/c)v(x, y, z)]^2/\Delta v^2} , \quad (4)$$

where the subscripts u and l refer to the upper and lower transition states, n represents the level populations, A and B are the Einstein coefficients, g is the statistical degeneracy, $v(x, y, z)$ is the local velocity of the emitting gas, and Δv is the line width.

The level populations n_u and n_l of the upper and lower states are assumed to be in statistical equilibrium, thus ensuring a

trivial consistency with the radiation field. Then given the temperature, the level populations may be determined from the partition function,

$$Q_n = \frac{g_n e^{-E-n/kT}}{\sum_{m=1}^{\infty} g_m e^{-E_m/kt}}, \quad (5)$$

and the number density and tracer abundance. The inputs to the model are therefore the three-dimensional velocity structure $v(x, y, z)$, the number density $n(H_2)(x, y, z)$, and the temperature $T(x, y, z)$. To compute a position-velocity diagram, the radiative transfer equation is integrated numerically over a line of points representing sky positions, and the model sky image is then convolved with a Gaussian equivalent to observing beam. This procedure is quite useful, as will be explained below, in illustrating the dependence of the spectral line shape on the source structure, particularly the velocity field. For dense gas such as that found in the molecular cores around H II regions, the LTE approximation has been found to provide a solution of sufficient accuracy to match the observational data to a level consistent with the noise in the data.

For a centrally condensed source, we use a logarithmic grid in the map plane, a linear grid in velocity, and an adaptive grid for the integration along the line of sight. When properly dimensioned, the grid is approximately linear in $e^{-\tau}$, where τ is the optical depth. The resulting image is then regridded in the map plane and convolved with the beam pattern and autocorrelator or filter bank response appropriate to the observing apparatus.

The scheme is flexible enough to handle a variety of simulations. In addition to the modeling of the accretion flow in G10.6−0.4 presented below, we have used the code to simulate an accretion flow in DR 21 (Keto 1990) with different parameters, and to compute the appearance of high-latitude colliding molecular clouds when observed in ^{13}CO with a single-dish antenna (Keto and Lattanzio 1989). In the latter case, we used the output from a three-dimensional smoothed-particle hydrodynamics calculation to specify the physical properties of the clouds. The code can also be extended in a straightforward way to include a non–LTE determination of the level populations using the Sobolev approximation. For a general velocity field one may, if warranted, ignore the coupling between multiple resonant points in the cloud, resulting in the so-called disconnected approximation, or correct for this effect by iteration (Marti and Noerdlinger 1977; Rybicki and Hummer 1978).

III. AN EXAMPLE: G10.6−0.4

a) *The Source*

The ultracompact H II region G10.6−0.4 is the brightest member of a complex of H II regions in an area of active star formation near the Galactic center. Spectral line observations of the dense gas immediately around the H II region suggest infall and rotation consistent with gravitational collapse in the potential well of the gas and stars. The flow represents a continuation beyond the onset of nuclear burning of the original accretion responsible for star formation. The rotational and infall velocities increase with decreasing radius suggesting spin-up and accelerating infall. Comparison of the $NH_3(1, 1)$ to $NH_3(3, 3)$ line ratios indicates that the molecular cloud core is heated by dust reradiation of the UV continuum from the newly formed stars and that the density is centrally condensed (Ho and Haschick 1986; Keto, Ho, and Haschick 1987, 1988).

b) *The Model*

Table 1 lists the equations and parameters which constitute the model. Table 2 lists some values of the physical quantities at representative radii. As stated in the introduction, the model, including the functional form, has been arbitrarily chosen on the basis of mathematical simplicity guided by the analysis of the observations in Keto, Ho, and Haschick (1987, 1988). The model is purely diagnostic in the sense that it is designed to match the observations rather than describe the physics of the accretion flow. In the sections below, we discuss the model in detail.

c) *A Comparison of the Images*

Our observations of G10.6−0.4 include four data sets. We observed the $NH_3(1, 1)$ and (3, 3) rotational states using a compact configuation (D) of the VLA to achieve 10″ resolution (Keto, Ho, and Haschick 1987), and an extended configuration (B) for 0.″3 resolution (Keto, Ho, and Haschick 1988). In Figures 1*a*–3*a* we plot the line brightness as a function of velocity and position in the equatorial plane of the rotating gas from three of these data sets. These position-velocity plots are useful for summarizing the dynamical information available in

TABLE 1

MODEL PARAMETERS

Parameter	Value
H II radius ($r_{H\,II}$)	0.025
Electron temperature (T_e)	8000 K
Continuum opacity ($\kappa_{H\,II}$)	3.25×10^{-18} cm^{-1}
Stellar mass (M_{st})	235 $M_\odot$
Systemic velocity (V_{LSR})	−3.5 km s^{-1}
Cloud radius (r_c)	1.0
Inclination angle (i)	0°
Ellipticity (ϵ)	1.0
Temperature [$T = T_0(r_T/r)^{\alpha_T}$]	$T_0 = 40$ K ($r_T = 0.35$; $\alpha_T = 0.5$)
Density [$n = n_0(r_n/r)^{\alpha_n}$]	$n_0 = 2 \times 10^4$ ($r_n = 0.35$; $\alpha_n = 2.5$)
Azimuthal velocity [$v_{az} = v_{0az}(r_{0az}/r)^{\alpha_{0az}} - v_{1az}(r/r_{1az})^{\alpha_{1az}}$]	$v_{0az} = 4.0$ ($r_{0az} = 0.025$; $\alpha_{0az} = 0.1$), $v_{1az} = 0.25$ ($r_{1az} = 0.025$; $\alpha_{1az} = 0.8$)
Turbulent velocity [$v_t = v_{0t}(r/r_{v_t})^{\alpha_v}$]	$v_{0t} = 0.25$ ($r_{v_t} = 0.025$; $\alpha_{v_t} = 0.8$)
Radial velocity [$v_r^2 = GM(r)/r - v_{az}^2 - v_t^2$]	...
[NH_3/H_2] (f_{NH_3})	1.4×10^{-6}

NOTES.—All radii are in pc. All velocities are in km s^{-1}.

TABLE 2

REPRESENTATIVE VALUES

Radius (pc)	log n (cm^{-3})	T (K)	v_r (km s^{-1})	v_{az} (km s^{-1})	log m ($M_\odot$)	log $\dot{m}$ $M_\odot$ yr^{-1}
H II[a]	5.1	8000	...	...	2.4	...
0.025	7.2	150	5.0	4.0	...	−2.6
0.1	5.6	75	3.4	3.4	2.8	−3.1
0.35	4.3	40	2.0	2.3	3.1	−3.6
1.0	3.2	24	0.0	0.0	3.3	0.0

[a] In the H II region, n refers to the electron density and m refers to the mass in ionized gas and stars. At other radii, n refers to the molecular density and m refers to the molecular mass within that radius.

the observations. The interpretation of these diagrams with respect to G10.6−0.4 is explained in § IV*f* below and in Keto, Ho, and Haschick (1987, 1988). [The high-resolution (3, 3) observations did not have a sufficient signal-to-noise ratio to be useful in the simulation.] In Figures 1*b*–3*b*, we show plots generated from our model. Spatial and spectral convolving functions equal to the beam and channel widths of the corresponding observations have been applied to each modeled image. The close correspondence between the observations and the model suggests a correspondence between the velocities, temperatures, and densities at all radii in the source and in the model.

d) H II *Region*

The parameters of the continuum, with the exception of the stellar mass, may be determined directly from the observations assuming a spherical H II region. The flux of UV photons required to ionize the observed H II region is 8×10^{50} (Haschick and Ho 1981) assuming a proton-to-dust ratio of 3100 (Spitzer 1978), and an order of magnitude lower with no dust. Because the stars are obscured by the overlying molecular cloud, it is not possible to determine the spectral type. Thus, alternative choices are fewer stars of earlier type resulting in a lower total stellar mass, or more stars of later type. The total luminosity is consistent with a few O stars or several later O and B. The numerical value of 235 $M_\odot$ was chosen to create a smooth gravitational potential in the molecular cloud just beyond the H II region boundary.

e) *Geometry*

Our model cloud is spherical with no inclination of the rotation axis; however, the observations can also be well modeled by a thick disk which is nearly edge-on, provided some adjustment to the density or size scale is also made. The position-velocity plots are not very sensitive to the inclination and ellipticity because modest changes affect the velocity and gravitational energy as scaling constants to a first approximation. For example, inclination of the rotation axis will change the apparent azimuthal velocity by sin i, and flattening of the cloud to a disk reduces the mass within any radius by about a factor equal to the ellipticity.

f) *Velocities*

There are three velocities in the model: radial, v_r, azimuthal, v_{az}, and turbulent, v_{turb}. The rotational velocity and the kinetic energy in turbulence are specified by power laws, and the infall velocity is computed from the constraint that the motions are gravitationally bound. Thus

$$v_r^2 = GM(r)/r - v_{az}^2 - v_{turb}^2 , \quad (6)$$

where $M(r)$ is the mass due to gas and stars within radius r. For conditions of constant total energy, the equation as written holds except that there might be additional terms on the right-hand side representing the gas pressure and the magnetic field. For the conditions described, low temperature and density, the gas pressure is negligible. One expects a strong magnetic field

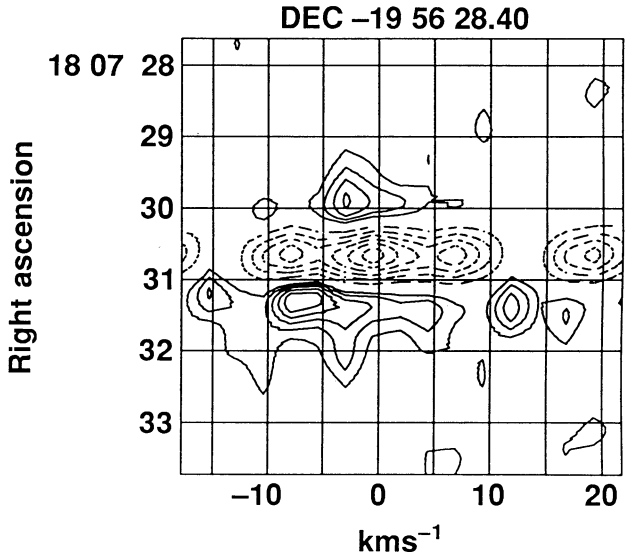

FIG. 1*a*

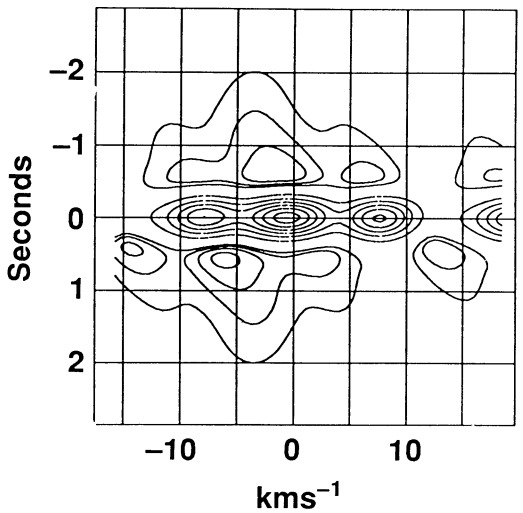

FIG. 1*b*

FIG. 1.—(*a*) Position-velocity plot of the $NH_3(1, 1)$ line brightness in the equatorial plane of G10.6−0.4. The resolution is 10″ and 2.4 km s^{-1}. Absorption is indicated by the dashed contours. The contour interval is 50 mJy $beam^{-1}$ in emission and 200 mJy $beam^{-1}$ in absorption. The multiple components are due to the hyperfine structure of NH_3. In absorption, the main hyperfine is at −0.5 km s^{-1} V_{LSR}; the two inner hyperfine satellites are symmetrically displaced by 7.8 km s^{-1}. The red outer hyperfine is at 19 km s^{-1}. The blue outer satellite is off the figure. The hyperfine structure may also be identified in emission. (*b*) Model position-velocity plot matching (*a*). The systemic velocity is −3.5 km s^{-1} V_{LSR}. The contour interval is 8.5 K in emission and 21 K in absorption.

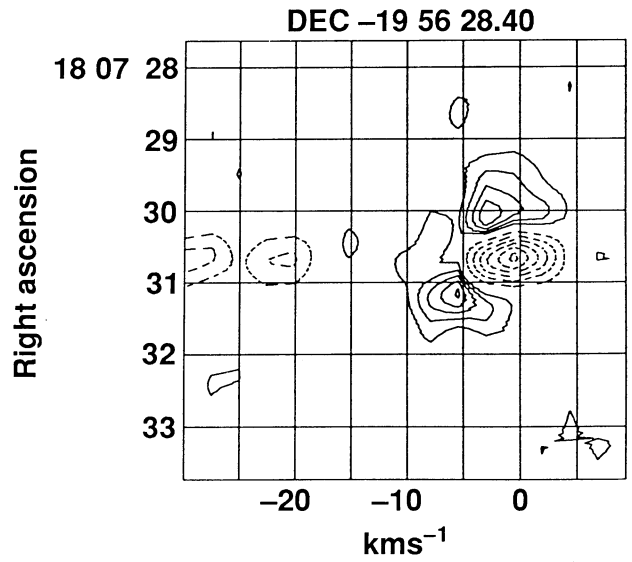

FIG. 2a

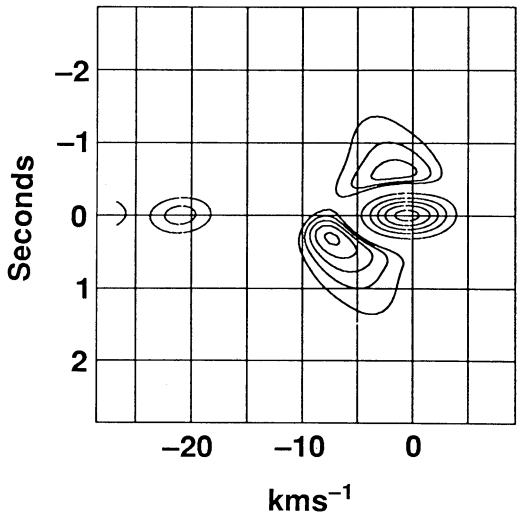

FIG. 2b

FIG. 2.—(*a*) Position-velocity diagram of the $NH_3(3, 3)$ line brightness in the same format as Fig. 1*a*. The contour interval is 75 mJy beam^{-1} in emission and 225 mJy beam^{-1} in absorption. The blue inner and outer hyperfine lines are visible in absorption at −22 and −29.4 km s^{-1} V_{LSR}. The red hyperfines are off the plot. (*b*) Model position-velocity plot of the $NH_3(3, 3)$ line brightness in the same format as Fig. 1*a*. The contour interval is 10 K in emission and 25 K in absorption.

in this source. This is discussed further below. Here we note that with the strong kinetic energies in the infall and rotational velocities, one does not expect the magnetic field strength to exceed equipartition with the velocities. Thus equation (6) should be good to within a factor of 2. The turbulent velocity serves two functions. First, it broadens the modeled lines to account for that part of the observed line width not attributable to the dynamics. Second, by increasing the random component of the velocity with increasing radius, it allows us to use the gravitational binding constraint above and to cut off the azimuthal and radial velocities at some radius. A plot of the three velocity components with radius is shown in Figure 4. In the paragraphs below, we describe each of the velocity components. A more detailed discussion of the interpretation of the velocity structure based on these position-velocity diagrams is given in Keto, Ho, and Haschick (1987, 1988).

The infall versus radius relation is determined by matching the progressive redshifting of the velocities at smaller radii in both Figures 1*a* and 3*a*. This is most evident in Figure 1*a* by the redshifting of the absorption and in Figure 3*a* by the curvature of the absorption trace across the position-velocity diagram. The absorption unambiguously places this gas in

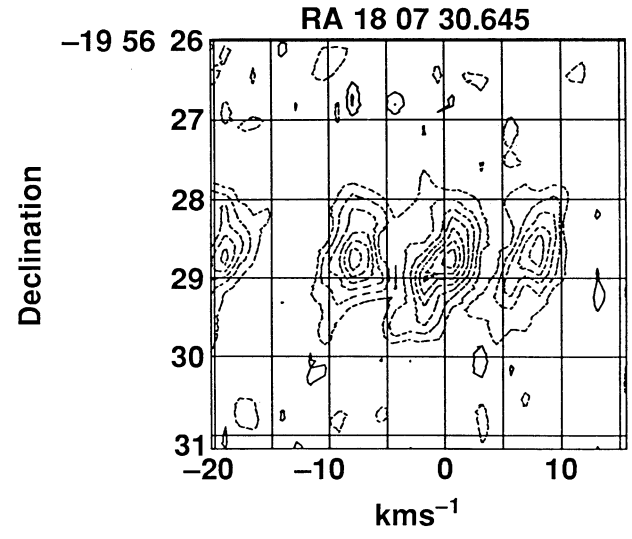

FIG. 3a

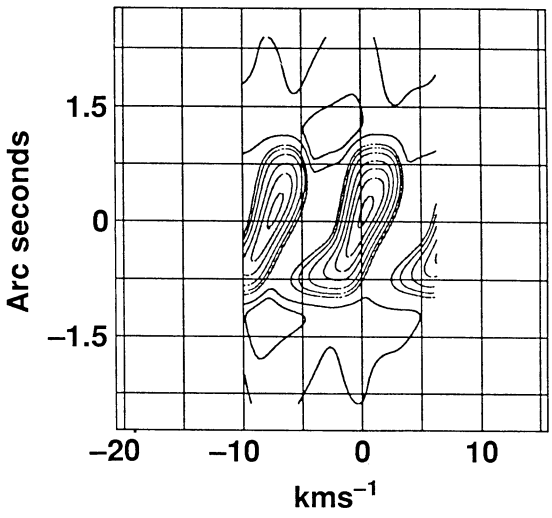

FIG. 3b

FIG. 3.—(*a*) Position-velocity diagram of the $NH_3(1, 1)$ line at 0.″4 and 1.2 km s^{-1} resolution. Dashed lines indicate absorption. The emission is below the sensitivity of this observation. The contour interval is 30 mJy beam^{-1}. (*b*) Model position-velocity diagram of the $NH_3(1, 1)$ line convolved to the same resolution as in (*a*). The contours are at −625, −500, −375, −250, −125, −62, −31, 12.5, and 25 K. Because the hyperfine lines are symmetric, only a portion of (*a*) has been modeled.

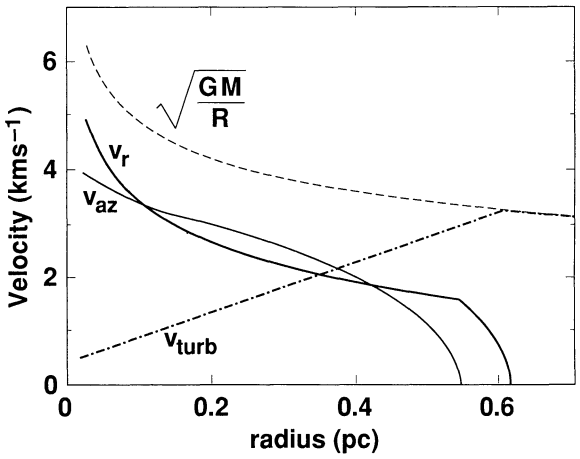

FIG. 4.—The three velocity components used in the model and the square root of the gravitational energy per unit mass plotted vs. radius.

front, as opposed to behind, the H II region. At radii less than 0.1 pc, the infall velocity scales as a low power of the radius $r^{-0.2}$. The cutoff in the radial velocity defining the outer boundary of the collapse zone is not well constrained in the sense that the radial and turbulent velocities at large radii may be traded off to a certain extent, one for the other. This is because the radial flow will split the line emission symmetrically about the systemic velocity on both sides of the H II region. Thus radial velocities less than our spectral resolution, 2.4 km s^{-1} at large scales, will not be readily distinguishable from turbulent broadening of similar magnitude.

The rotation curve is determined by matching the varying red-blue asymmetry of the velocities with radial distance on either side of the H II region center in Figures 1*a* and 1*c*. Over most of the collapse zone $\Omega \sim r^{-1}$ (Fig. 5). The cutoff in the rotational velocity at about 0.5 pc is well constrained by the emission at -3.5 km s^{-1} seen in Figure 1*a* on both sides of the H II region beyond 0.5 pc. The fact that this emission is the same on both sides of the H II region implies that gas at this radius is not involved in the rotation. Significant rotation at this radius would shift this emission blueward and redward approximately by the rotational velocity $v_{az} = \Omega r$.

The model shown here has a turbulent velocity increasing as $r^{0.8}$ from less than 0.5 km s^{-1} inside of 0.1 pc to a value

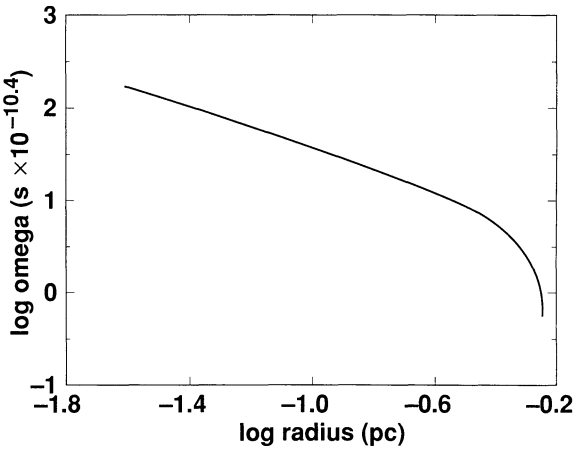

FIG. 5.—Angular velocity in s^{-1} vs. radius

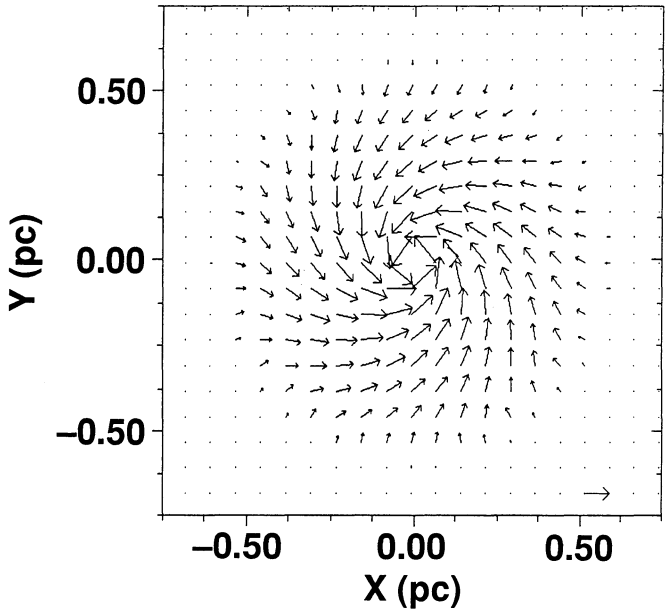

FIG. 6.—The velocity directions and magnitudes in the equatorial plane of the accretion flow. The arrow in the lower right corresponds to 1.3 km s^{-1}.

consistent with the turbulent broadening away from the collapse center ~ 3 km s^{-1}.

Figure 6 shows a vector plot of the modeled velocities in the equatorial plane. The gas spirals into the center quite rapidly, completing less than one orbit over the two decades in radial distances accessible by the observations. The failure to achieve rotational support suggests either collapse from a state of negligibly low angular momentum, or more likely, strong angular momentum braking. Although our model does not constrain the collapse evolution, we may estimate the braking torque required to maintain the present observed low angular momentum distribution over an infall time scale. The time rate of change of the angular momentum may be estimated as $dL/dt = mv_r(v_{az1}r_1 - v_{az2}r_2)/(r_1 - r_2)$. To be correct, we need the value of v_{az1} at time $t - dt$, which is not available from our data. Our estimate therefore strictly applies only assuming a steady state velocity field which we know cannot be correct (see § IV*h*). Nevertheless, using the numbers from Table 2, the required torque is about 5×10^{46} ergs from 0.35 to 0.1 pc and 10^{47} ergs from 0.1 to 0.025 pc. A rough estimate of the magnetic field strength required to provide the braking torque by Maxwell stress may be determined by comparing the average magnetic energy over the volume of the collapse $\langle B^2/8\pi \rangle$, with the torque. The average field strength within 0.35 pc is 0.5 mG and is a factor of 10 higher within 0.1 pc. The required field strengths are within the range measured by Zeeman splitting of OH masers in other dense molecular cloud cores around similar H II regions. The increase in field strength at small radii is also consistent with the increase expected from flux freezing as the number density increases by three orders of magnitude over the condensed core.

g) Tracer Abundance

We have used the velocities, which are the most tightly constrained of our parameters, together with the gravitational binding constraint to fix the number density of H_2. Given this density and the observed optical depth of our tracer, NH_3,

allows us to determine the abundance ratio $[NH_3/H_2]$. Our model indicates a ratio of 1.4×10^{-6}. The uncertainty, although difficult to estimate, should be on the order of a factor of a few (§ IV*i*).

h) Temperature and Density

The number density of H_2 is determined mainly from the constraint that the kinetic energy in the modeled velocities be equal to the gravitational binding energy at each radius. The total kinetic energy is well constrained and discussed in § IV*f* above. It should be noted that the cloud collapse is not in steady state; thus the mass flux is not constrained to be constant with radius. We expect the mass flux to be decreasing with radius consistent with star formation in inside-out collapse (Shu, Adams, and Lizano 1987). Values for $\dot{m}$ at several radii are listed in Table 2. The typical rate of $10^{-3}\ M_\odot\ \mathrm{yr}^{-1}$ over the infall time scale of 10^5 yr will accrete 200 $M_\odot$ of gas, approximately the same as the estimated stellar mass. The infall time scale is set very approximately by the observation that there are characteristically several ultracompact H II regions in one star-forming region. Since the lifetime of a massive star is approximately 10^6 yr, the formation time should be shorter, or previously formed massive stars would have gone supernova. The lower bound is determined by the free-fall time scale, 10^4 or 10^5 depending on the local density.

The response of the LTE model to increasing temperature is described by the partition function and is to adjust the level populations to higher excitation energies. Thus, once having fixed the run of $NH_3(1, 1)$ density with radius using the constraints on the velocities and tracer abundance, the temperature versus radius relation may be determined by matching the ratio of the (3, 3) to (1, 1) optical depths which themselves are given in Figures 1*b* and 2*b* by the main-to-satellite hyperfine ratios of each of the respective lines. A more detailed discussion of the interpretation of temperature is given in Keto, Ho, and Haschick (1987).

Physically, we expect that the UV flux from the stars is absorbed by dust grains in the molecular cloud which in turn heat the gas through collisions. The heat flow through the cloud can be shown to result in a dust temperature gradient scaling as $T \sim r^{-1/4}$ to $r^{-1/5}$ (Scoville and Kwan 1976). At lower densities, $n < 10^5$, the gas partially uncouples from the dust, implying a higher gas temperature gradient. Our model suggests that $T \sim r^{-1/2}$ may be appropriate.

i) Errors

For a comparison between a particular model and data, one would like to estimate in an objective way the usefulness of the comparison. Most techniques for error estimation would involve multiple independent radiative transfer simulations, varying the parameters of the simulations and comparing the solutions with the data. There are two difficulties: (1) Such multiple solutions of a three-dimensional radiative transfer simulation are beyond the computational budget of the current project; (2) Even such a detailed analysis may not answer the question we are posing. Although we can examine the effect of varying the parameters of a model, we cannot express the uncertainties related to the nonuniqueness or arbitrary choice of the model used in the solution. This unavoidable nonuniqueness arises because of the projection effects associated with astronomical observations. That is, the projection of the three-dimensional source structure onto the two-dimensional sky image and the projection of the three-dimensional velocity structure onto the line of sight leaves us with insufficient information to specify the full three-dimensional model. Because the information is missing, the parameterization must be derived from considerations outside the data—symmetry, smoothness, sensible physics. However, the information required to estimate the appropriateness of our choice of parameterization is also missing.

An informal but reasonably sensible approach to adopt is to assume that: (1) The errors in the derived velocities are on the order of the channel width, (2) the errors in position are on the order of the beam size, (3) features below a few times the noise level are not significant. The relevant channel widths, beam sizes, and noise levels are 2.4 km s^{-1}, 10″, and 20 mJy $beam^{-1}$ for the lower angular resolution observations and 1.2 km s^{-1}, 0″.3, and 40 mJy $beam^{-1}$ for the higher resolution observations. An analysis of errors for simplified forms of the radiative transfer equations in Keto, Ho, and Haschick (1987, 1988) suggests that the derived quantities such as temperature and density are known to within factors of about 1.5–2. Thus, power-law exponents should be accurate to within the range ± 0.3 to ± 0.5. Despite the simplicity of this approach, this estimate of the errors should be reasonably accurate. The estimate is exact in the case where the underlying error distribution is Gaussian normal and the equations are sufficiently linear that the propagation of errors results in a symmetric distribution. Of course, the radiative transfer equations are only close to linear in the optically thin approximation which does not hold throughout the model, but this estimate represents the best linear approximation. Second, this estimate is based solely on the data and the observational parameters and is therefore independent of the choice or structure of the model. Of course, one needs the model itself to interpret the analysis, but the error estimate would not change for a different choice of model.

IV. CONCLUSIONS

Our results suggest that the model and the radiative transfer solution are sufficiently detailed to describe the source and the observations and that satisfactory results are obtainable even at the modest signal-to-noise ratios, between 5:1 and 10:1 typical of high-resolution VLA NH_3 data. The modeling applied to G10.6−0.4 shows an accretion flow in a strongly condensed ($n \sim r^{-2.5}$) molecular cloud core. The rotation curve ($\Omega \sim r^{-1}$) and rapid infall velocities ($v_r \sim v_{az}$) suggest either collapse from an initial state of negligibly low angular momentum or rapid transfer of angular momentum during the collapse.

The author acknowledges the assistance and encouragement of W. Jeffrey and R. Rosner, who have contributed to the understanding of this problem through many questions and suggestions. Work performed under the auspices of U.S. Department of Energy at Lawrence Livermore National Laboratory under contract number W-7405-ENG-48.

REFERENCES

Guesten R., Genzel, R., Wright, M. C. H., Jaffe, D. T., Stutzki, J., and Harris, A. I. 1987, *Ap. J.*, **318**, 124.
Haschick, A. D., and Ho, P. T. P. 1981, *Ap. J.*, **248**, 622.
Ho, P. T. P., and Haschick, A. D. 1986, *Ap. J.*, **304**, 501.
Keto, E. R. 1990, *Ap. J.*, in press.
Keto, E. R., Ho, P. T. P., and Haschick, A. D. 1987, *Ap. J.*, **318**, 712.

Keto, E. R., Ho P. T. P., and Haschick, A.D. 1988, *Ap. J.*, **324**, 920.
Keto, E. R., and Lattanzio, J. H. 1989, *Ap. J.*, **346**, 184.
Marti, F., and Noerdlinger, P. D. 1977, *Ap. J.*, **215**, 247.
Rybicki, G. B., and Hummer, D. G. 1978, *Ap. J.*, **219**, 654.
Sargent, A., and Beckwith, S. 1987, *Ap. J.*, **323**, 294.
Scoville, N., and Kwan, J. 1976, *Ap. J.*, **215**, 247.
Shu, F. H., Adams, F. C., and Lizano, S. 1987, *Ann. Rev. Astr. Ap.*, **25**, 23.
Spitzer, L. 1978, *Physical Processes in the Interstellar Medium* (New York: Wiley–Interscience).

E. KETO: Institute of Geophysics and Planetary Physics, Lawrence Livermore National Laboratory, P.O. Box 808-L413, Livermore, CA 94550